ELSEVIER

International Journal of Solids and Structures 41 (2004) 2277–2292

INTERNATIONAL JOURNAL OF SOLIDS and STRUCTURES

www.elsevier.com/locate/ijsolstr

An incremental algorithm for static shape control of smart structures with nonlinear piezoelectric actuators

Dongchang Sun [a,*], Liyong Tong [a,*], Dajun Wang [b]

[a] School of Aerospace, Mechanical and Mechatronic Engineering, The University of Sydney, Sydney, NSW 2006, Australia
[b] Department of Mechanics and Engineering Science, Peking University, Beijing 100871, China

Received 5 December 2003; received in revised form 5 December 2003

Abstract

Optimum control voltage design for static shape control of structures with nonlinear piezoelectric actuators is studied in this paper. In order to perform static shape control, the finite element equations of plates with nonlinear piezoelectric actuator patches is formulated using an eight-node adhesive element which combines a pair of collocated four-node quadrilateral elements for the upper and lower plates and a pseudo-adhesive layer element. An iteratively calibrated incremental method is presented to find the optimal control voltages that can actuate a shape best matching the desired shape. In this method, the desired shape is expressed by the sum of a number of small incremental desired shapes, and the control voltages to achieve each incremental desired shape are calculated step by step. The control voltages in each step are then calibrated by using the accumulated intermediate desired shape iteratively. Finally, a simulation example is given to illustrate that the present algorithm is effective in finding the optimal control voltage distribution for shape control of nonlinearly actuated structures. The results show that the present method can give satisfactory control voltages with a reasonable number of incremental steps.

Keywords: Shape control; Piezoelectric transducers; Nonlinear; Adhesive element; Incremental algorithms

1. Introduction

Static shape control of flexible structures using piezoelectric actuators has attracted much attention in recent years (Irschik, 2002; Tong et al., 1998; Ghosh and Batra, 1995; Bruch et al., 2000). The main task in static shape control of structures using piezoelectric actuators is to design the control voltages so as to achieve or best match the desired shape. Since the shape control of structures is an inverse problem, except for several simple structures, the control voltages cannot be solved uniquely. Static shape control can be performed based on analytical solutions (Zhang and Sun, 1999; Vel and Batra, 2001) for some structures. However, due to the difficulties in seeking the analytical solutions for more complicated structures, the control voltages are usually sought using finite element analysis (FEA) (Benjeddou et al., 1999) and

* Corresponding authors. Tel.: +61-2-93518021; fax: +61-2-93514841.
E-mail addresses: dsun@aeromech.usyd.edu.au (D. Sun), ltong@aeromech.usyd.edu.au (L. Tong).

0020-7683/$ - see front matter © 2003 Elsevier Ltd. All rights reserved.
doi:10.1016/j.ijsolstr.2003.12.002

optimization procedures to minimize the difference between the actuated shape and the desired one. The optimal control voltages can be obtained either analytically or numerically. Koconis et al. (1994) developed a solution scheme to find the optimal control voltages by minimizing an error function between the deformed shape and the desired shape. Hsu et al. (1997) applied the gradient projection algorithm to find the optimal values of design variables in the shape control of plates. Agrawal and Treanor (1999) employed the simplex search algorithm to find the optimal actuator locations and voltages. Recently, Chee et al. considered more general error functions including curvatures (Chee et al., 2001) and slopes (Chee et al., 2002) and presented procedures to find the optimal voltage distribution in static shape control of smart plates based on numerical optimization methods.

In most cases, the constitutive relation of piezoelectric materials is nonlinear (Wang et al., 1999) and may even exhibit hysteresic behavior (Zhou and Chattopadhyay, 2001) under a cyclic electric field. Although there are many literatures (Agnes and Inman, 1996; Zhou and Tzou, 2000) referring to the nonlinear piezoelectric materials, the research on shape control of structures using nonlinear piezoelectric actuators is very rare. Ajit et al. (2001) presented a feedback algorithm (FA) for shape control of beams with nonlinear piezoelectric actuators. In this method, the actuation voltages required for shape control are estimated by an incremental procedure, and then the difference between the actuated shape and the desired one is calculated. If this difference is not small enough, it is taken as the new desired shape and repeat the same process until the final control voltages is obtained.

In this paper, an iteratively calibrated incremental method (ICIM) is presented to find the optimal control voltages for static shape control of structures with nonlinear piezoelectric actuators. The basic equation used for shape control is formulated based on an adhesive element model, which includes a four-node quadrilateral upper plate element, a lower plate elements and a thin adhesive layer element. To find the optimal control voltages, the desired shape is divided into a number of small incremental desired shapes, and the control voltages to achieve each incremental desired shape are estimated in each incremental step. The control voltages in each step then are calibrated iteratively by using the accumulated intermediate desired shape. In addition to the ICIM, other methods such as simple incremental method (SIM), iterative incremental method (IIM), and calibrated incremental method (CIM) are also formulated and evaluated by comparing them with the FA. Finally, a simulation example is given to illustrate the present method. The results show that the present method can give satisfactory control voltages for shape control of nonlinearly actuated structures with a reasonable number of incremental steps.

2. Basic equations of plates with nonlinear piezoelectric actuators

2.1. Description of nonlinear piezoelectricity

The nonlinear constitutive relation may be expressed in the following form:

$$\boldsymbol{\sigma} = \mathbf{C}\boldsymbol{\varepsilon} - \boldsymbol{\sigma}_p(\mathbf{E}), \tag{1}$$

where $\boldsymbol{\sigma} \in R^6$ and $\boldsymbol{\varepsilon} \in R^6$ are the stress and strain vector, respectively; $\mathbf{C} \in R^{6\times 6}$ is the elastic matrix and $\boldsymbol{\sigma}_p(\mathbf{E}) \in R^6$ is the stress induced by the nonlinear piezoelectricity which are nonlinear functions of the applied electric field $\mathbf{E} \in R^3$. The nonlinear stress can be rearranged into the following form:

$$\boldsymbol{\sigma}_p(\mathbf{E}) = \mathbf{e}^{\mathrm{T}}(\mathbf{E})\mathbf{E}, \tag{2}$$

where $\mathbf{e}(\mathbf{E}) \in R^{3\times 6}$ is the piezoelectric stress coefficient matrix, whose entries can be expressed as functions of the applied electric field density for nonlinear piezoelectric materials (Crawley and Lazarus, 1991; Tan and Tong, 2001). In general, each entry of the piezoelectric stress coefficient matrix can be approximated by the first several terms of its Taylor expansion.

When both direct and inverse piezoelectric effects are taken into account, the *e*-type constitutive relation of a nonlinear piezoelectric material can be descried by

$$\begin{aligned} \boldsymbol{\sigma} &= \mathbf{C}\boldsymbol{\varepsilon} - \mathbf{e}^{\mathrm{T}}(\mathbf{E})\mathbf{E}, \\ \mathbf{D} &= \mathbf{e}(\mathbf{E})\boldsymbol{\varepsilon} + \boldsymbol{\eta}\mathbf{E}, \end{aligned} \tag{3}$$

where $\boldsymbol{\eta} \in R^{3\times 3}$ is the permittivity matrix, $\mathbf{D} \in R^3$ is the electric displacement vector. For a nonpiezoelectric material, $\mathbf{e}$ and $\boldsymbol{\eta}$ are zero matrices.

2.2. Finite element formulation

In this section, the basic equations are formulated for static shape control of plates with nonlinear piezoelectric actuator patches (see Fig. 1) based on an eight-node adhesive element. To form the finite element equations of the composite plate bonded with nonlinear piezoelectric actuator/sensor patches, an adhesive element is employed, which includes collocated four-node quadrilateral elements for the upper and lower adherents and a pseudo-adhesive layer element, as shown in Fig. 2.

For the upper and lower elements in the adhesive element, four-node isoparametric elements with five degrees of freedom at each node are used. Denoting $\mathbf{u} = (u, v, w, \psi_x, \psi_y)^{\mathrm{T}}$ which consists of the translational displacements and the rotational angle about x- and y-axes in the upper and lower plate elements, the displacement vector can be expressed in the form of interpolation:

$$\mathbf{u}_i(x, y) = \mathbf{N}(x, y)\mathbf{u}_i^{\mathrm{e}}, \quad i = 1, 3, \tag{4}$$

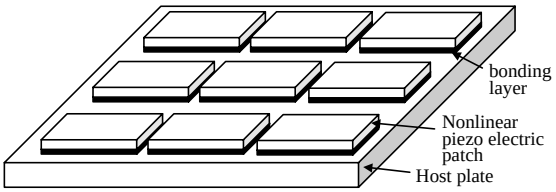

Fig. 1. Plate with nonlinear piezoelectric actuator patches.

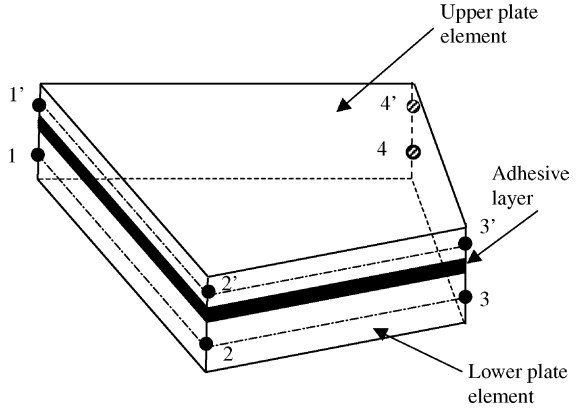

Fig. 2. An eight-node adhesive element with upper, lower adherents and bonding layer.

where the subscript $i(=1,2,3)$ represents the upper, adhesive and low plate elements, respectively, $\mathbf{u}_i^e$ is a vector consisting of the displacements at four nodes of the element, $\mathbf{u}_i^e = \left(\mathbf{u}_{i1}^T \quad \mathbf{u}_{i2}^T \quad \mathbf{u}_{i3}^T \quad \mathbf{u}_{i4}^T\right)^T$ and $\mathbf{u}_{ij}^T$ $(j=1,2,3,4)$ is the nodal displacement vector at the jth node of the ith element. The matrix $\mathbf{N}$ is the interpolation matrix given by

$$\mathbf{N} = [\mathbf{N}_1 \quad \mathbf{N}_2 \quad \mathbf{N}_3 \quad \mathbf{N}_4], \quad \mathbf{N}_j = N_j \mathbf{I}_5, \quad N_j(\xi,\eta) = (1+\xi_j\xi)(1+\eta_j\eta)/4, \qquad j=1,2,3,4, \tag{5}$$

where (ξ_j, η_j) is the coordinates of the jth node in the parent element. In addition, to avoid shear locking problem, the shape functions for the two rotational angles are replaced by (Tong and Sun, 2000)

$$N_{\xi j} = (1-\eta_j\eta)/4, \quad N_{\eta j} = (1-\xi_j\xi)/4, \qquad j=1,2,3,4 \tag{6}$$

which are used to calculate the shear strain ε_{yz} and ε_{xz}.

Employing Eq. (4), the strains in the upper and lower elements can be expressed in terms of the nodal displacements as follows:

$$\bar{\varepsilon}_i = \mathbf{B}_i \mathbf{u}_i^e, \quad i=1,3, \tag{7}$$

where $\mathbf{B}_i \in R^{8\times 20}$ is the strain–displacement matrix, $\bar{\boldsymbol{\varepsilon}}_i = (\boldsymbol{\varepsilon}_{bi}^T \quad \boldsymbol{\chi}_i^T \quad \boldsymbol{\varepsilon}_{si}^T)^T$ is the generalized strain vector in which $\boldsymbol{\varepsilon}_{bi} = (\varepsilon_{xx}, \varepsilon_{yy}, \gamma_{xy})_i^T$, $\boldsymbol{\chi}_i = (\chi_{xx}, \chi_{yy}, \chi_{xy})_i^T$ and $\boldsymbol{\varepsilon}_{si} = (\gamma_{yz}, \gamma_{xz})_i^T$ are the membrane, bending and shear strains, respectively.

The strains in the adhesive layer between the upper and lower elements can be also expressed by the eight nodal displacement vectors. Since the adhesive layer is very thin, we assume that it carries constant shear strains γ_{yz}, γ_{xz} and peel strain ε_z along its thickness and the other strains ε_x, $\boldsymbol{\varepsilon}_y$ and γ_{xy} can be neglected. The shear and peel strains in the adhesive layer element can be expressed as

$$\begin{aligned}
\varepsilon_{z2} &= (w_1 - w_3)/h_2, \\
\gamma_{yz2} &= \left(v_1 - v_3 + \frac{h_1}{2}\psi_{x1} + \frac{h_3}{2}\psi_{x3}\right)\Big/ h_2, \\
\gamma_{xz2} &= \left(u_1 - u_3 - \frac{h_1}{2}\psi_{y1} - \frac{h_3}{2}\psi_{y3}\right)\Big/ h_2,
\end{aligned} \tag{8}$$

where the subscript 2 represents the adhesive layer, ψ_x and ψ_y are the rotational angle about axes y and x, respectively. Substituting Eq. (4) into Eq. (8), the strain vector in the adhesive layer can be expressed by

$$\boldsymbol{\varepsilon}_2 = \mathbf{L}_{a1}\mathbf{N}\mathbf{u}_1^e + \mathbf{L}_{a3}\mathbf{N}\mathbf{u}_3^e, \tag{9}$$

where

$$\boldsymbol{\varepsilon}_2 = \begin{bmatrix} \boldsymbol{\varepsilon}_{z2} \\ \gamma_{yz2} \\ \gamma_{xz2} \end{bmatrix}, \quad \mathbf{L}_{ai} = \frac{1}{2h_2}\begin{bmatrix} 0 & 0 & 2 & 0 & 0 \\ 0 & 2 & 0 & h_i & 0 \\ 2 & 0 & 0 & 0 & -h_i \end{bmatrix}, \qquad i=1,3. \tag{10}$$

In addition to the mechanical degrees of freedom (DOF), the electric potential in a plate element should also be considered. It is assumed that the electric potential is linearly distributed in the piezoelectric actuator layer along its thickness and that the potential at its bottom is set to be zero. In this case, the potential at the upper surface is equal to the applied voltage between its two electrodes. Similar to the treatment of mechanical DOF, the electric potential (voltage) in a plate element can be expressed by its four nodal voltages using the same shape functions as the mechanical degrees, i.e.,

$$V_i = \mathbf{N}_E \mathbf{v}_i^{\mathrm{e}}, \quad i = 1, 3, \tag{11}$$

where $\mathbf{v}_i^{\mathrm{e}} \in R^4$ is a vector consisting of the four nodal voltages for element e, and $\mathbf{N}_E = [N_1 \quad N_2 \quad N_3 \quad N_4]$. The electric field densities along x, y and z directions can be obtained by differentiating the potential with respect to x, y and z, respectively and can be written in the following form:

$$\mathbf{E}_i = -\mathbf{B}_{Ei} \mathbf{v}_i^{\mathrm{e}}, \quad i = 1, 3, \tag{12}$$

where

$$\mathbf{B}_{Ei} = \mathbf{L}_{Ei} \mathbf{N}_E, \quad \mathbf{L}_{Ei}(z) = \frac{1}{h_i} \begin{pmatrix} z\frac{\partial}{\partial x} & z\frac{\partial}{\partial y} & 1 \end{pmatrix}^{\mathrm{T}}, \quad i = 1, 3. \tag{13}$$

The total strain and electric energy of an adhesive element can be written as

$$U = \frac{1}{2} \sum_{i=1,3} \int_{V_i} \left(\boldsymbol{\varepsilon}_i^{\mathrm{T}} \boldsymbol{\sigma}_i - \mathbf{D}_i^{\mathrm{T}} \mathbf{E}_i \right) \mathrm{d}V + \frac{1}{2} \int_{V_2} \boldsymbol{\varepsilon}_2^{\mathrm{T}} \boldsymbol{\sigma}_2 \, \mathrm{d}V, \tag{14}$$

where V_i is the volume occupied by the ith element. Using the generalized strain vector, the energy of an adhesive element can be further expressed as

$$U = \frac{1}{2} \sum_{i=1,3} \int_{V_i} \left[\bar{\boldsymbol{\varepsilon}}_i^{\mathrm{T}} \bar{\mathbf{C}}_i \bar{\boldsymbol{\varepsilon}}_i - 2 \bar{\boldsymbol{\varepsilon}}_i^{\mathrm{T}} \bar{\mathbf{e}}_i(\mathbf{E}_i) \mathbf{E}_i - \mathbf{E}_i^{\mathrm{T}} \boldsymbol{\eta}_i \mathbf{E}_i \right] \mathrm{dV} + \frac{1}{2} \int_{A_2} \boldsymbol{\varepsilon}_2^{\mathrm{T}} \mathbf{C}_2 \boldsymbol{\varepsilon}_2 \, \mathrm{d}V, \tag{15}$$

$$\bar{\mathbf{C}}_i = \begin{bmatrix} \mathbf{C}_{bi} & z\mathbf{C}_{bi} & \mathbf{0} \\ z\mathbf{C}_{bi} & z^2\mathbf{C}_{bi} & \mathbf{0} \\ \mathbf{0} & \mathbf{0} & \mathbf{C}_{si} \end{bmatrix}, \quad \bar{\mathbf{e}}_i = \begin{bmatrix} \mathbf{e}_b^{\mathrm{T}} \\ z\mathbf{e}_b^{\mathrm{T}} \\ \mathbf{e}_s^{\mathrm{T}} \end{bmatrix}_i, \quad \mathbf{C}_2 = \begin{bmatrix} c_{33} & 0 & 0 \\ 0 & c_{44} & 0 \\ 0 & 0 & c_{55} \end{bmatrix}_2,$$

$$\mathbf{C}_{bi} = \begin{bmatrix} c_{11} & c_{12} & c_{16} \\ c_{12} & c_{22} & c_{26} \\ c_{16} & c_{26} & c_{66} \end{bmatrix}_i, \quad \mathbf{C}_{si} = \begin{bmatrix} c_{44} & 0 \\ 0 & c_{55} \end{bmatrix}_i, \quad \mathbf{e}_{bi} = \begin{bmatrix} e_{11} & e_{12} & e_{16} \\ e_{21} & e_{12} & e_{26} \\ e_{31} & e_{32} & e_{36} \end{bmatrix}_i, \quad \mathbf{e}_{si} = \begin{bmatrix} e_{14} & e_{15} \\ e_{24} & e_{25} \\ e_{34} & e_{35} \end{bmatrix}_i. \tag{16}$$

Note that $\bar{\mathbf{e}}_i, \mathbf{e}_{bi}$ and $\mathbf{e}_{si}$ are no longer constant matrices but electric field-dependent matrices for the piezoelectric materials with nonlinear piezoelectricity.

The work done by external mechanical loads is given by

$$W = \sum_{i=1,3} \left(\mathbf{u}_i^{\mathrm{eT}} \mathbf{F}_{ci} + \int_{S_i} \mathbf{u}_i^{\mathrm{T}} \mathbf{f}_{si} \, \mathrm{dS} + \int_{V_i} \mathbf{u}_i^{\mathrm{T}} \mathbf{f}_{Vi} \, \mathrm{dV} \right), \tag{17}$$

where $\mathbf{F}_{ci}$ is the concentrated force vector, $\mathbf{f}_{si}$ and $\mathbf{f}_{Vi}$ are the surface and volume force vector, respectively.

Employing the principle of virtual work, the following equilibrium equations for each adhesive element can be obtained:

$$\mathbf{K}^{\mathrm{e}} \mathbf{u}^{\mathrm{e}} + \mathbf{g}^{\mathrm{e}}(\mathbf{v}^{\mathrm{e}}) = \mathbf{F}^{\mathrm{e}}, \tag{18}$$

where $\mathbf{u}^{\mathrm{e}} = \begin{pmatrix} \mathbf{u}_1^{\mathrm{eT}} & \mathbf{u}_3^{\mathrm{eT}} \end{pmatrix}^{\mathrm{T}}$ and $\mathbf{v}^{\mathrm{e}} = \begin{pmatrix} \mathbf{v}_1^{\mathrm{eT}} & \mathbf{v}_3^{\mathrm{eT}} \end{pmatrix}^{\mathrm{T}}$ are the nodal displacement and voltage vectors of the adhesive element including both upper and lower plate elements, and

$$\mathbf{K}^{\mathrm{e}} = \begin{bmatrix} \mathbf{K}_1^{\mathrm{e}} + \mathbf{K}_{a11} & \mathbf{K}_{a13} \\ \mathbf{K}_{a13} & \mathbf{K}_3^{\mathrm{e}} + \mathbf{K}_{a33} \end{bmatrix}, \quad \mathbf{g}^{\mathrm{e}}(\mathbf{v}^{\mathrm{e}}) = \begin{Bmatrix} \mathbf{g}_1(\mathbf{v}_1^{\mathrm{e}}) \\ \mathbf{g}_2(\mathbf{v}_2^{\mathrm{e}}) \end{Bmatrix}, \quad \mathbf{F}^{\mathrm{e}} = \begin{Bmatrix} \mathbf{F}_{c1}^{\mathrm{e}} + \mathbf{F}_{s1}^{\mathrm{e}} + \mathbf{F}_{V1}^{\mathrm{e}} \\ \mathbf{F}_{c3}^{\mathrm{e}} + \mathbf{F}_{s3}^{\mathrm{e}} + \mathbf{F}_{V3}^{\mathrm{e}} \end{Bmatrix} \tag{19}$$

and

$$\mathbf{K}_i^{\mathrm{e}} = \int_{V_i} \mathbf{B}_i^{\mathrm{T}} \overline{\mathbf{C}}_{\mathbf{i}} \mathbf{B}_{\mathbf{i}} \, \mathrm{d}\mathbf{V}, \quad \mathbf{g}_{\mathbf{i}}(\mathbf{v}_{\mathbf{i}}^{\mathrm{e}}) = \left(\int_{\mathbf{V_i}} \mathbf{B}_{\mathbf{i}}^{\mathrm{T}} \bar{\mathbf{e}}_{\mathbf{i}}(\mathbf{v}_{\mathbf{i}}^{\mathrm{e}}) \mathbf{B}_{\mathbf{Ei}} \, \mathrm{d}\mathbf{V} \right) \mathbf{v}_{\mathbf{i}}^{\mathrm{e}}, \quad \mathbf{F}_{\mathbf{si}}^{\mathrm{e}} = \int_{\mathbf{S_i}} \mathbf{N}^{\mathrm{T}} \mathbf{f}_{\mathbf{si}} \, \mathrm{d}\mathbf{S},$$

$$\mathbf{F}_{Vi}^{\mathrm{e}} = \int_{V_i} \mathbf{N}^{\mathrm{T}} \mathbf{f}_{Vi} \, \mathrm{d}V, \quad \mathbf{K}_{aij} = \int_{V_2} \mathbf{N}^{\mathrm{T}} \mathbf{L}_{ai}^{\mathrm{T}} \mathbf{C}_2 \mathbf{L}_{aj}^{\mathrm{T}} \mathbf{N} \, \mathrm{d}V, \qquad j = 1,3, \;\; i = 1,3. \tag{20}$$

Eq. (18) gives the equilibrium equations for an adhesive element which couples the nodal displacements and the nodal voltages in both upper and lower plate elements. Since an adhesive element layer has eight nodes and there are five mechanical DOF and one electric DOF in each node, Eq. (18) gives 40 equations consisting of 40 mechanical DOF and eight electric DOF (voltage). $\mathbf{K}_{aij}$ $(i,j = 1,3)$ in Eq. (20) is the contributions of the adhesive layer to the element stiffness matrix $\mathbf{K}^{\mathrm{e}}$.

The global equations for a smart plate can be obtained by assembling the element equations given in Eq. (18). The global equilibrium equations of a plate with nonlinear piezoelectric actuator can be written into the following general form:

$$\mathbf{K}\mathbf{u} + \mathbf{g}(\mathbf{v}) = \mathbf{f}, \tag{21}$$

where $\mathbf{K} \in R^{n \times n}$ is the global stiffness matrix, $\mathbf{g}(\mathbf{v}) \in R^n$ is a vector of control forces whose components are nonlinear functions of the control voltage, $\mathbf{v} \in R^{n_V}$, the voltage vector composed of all nodal voltage of the piezoelectric actuators, $\mathbf{u} \in R^n$ is the displacement vector consisting of all nodal displacements, $\mathbf{f} \in R^n$ is the force vector contributed by all mechanical loads, n and n_V are the total numbers of mechanical and electric DOF, respectively.

2.3. Error function for shape control

To generally measure the closeness between an actuated shape and a desired shape, consider a generalized "shape" defined by

$$\mathbf{y} = \mathbf{R}\mathbf{u}, \tag{22}$$

where $\mathbf{R} \in R^{m \times n}$ is a weighting matrix, and $\mathbf{y} \in R^m$ is an index vector. The generalized shape can be displacement, slope, curvature, strain, generalized force or their combination depending on the selection of the weighting matrix $\mathbf{R}$.

To find the optimal control voltages for the actuator patches, an error function between the actuated shape and the desired shape must be defined. For a given desired shape $\mathbf{y}_d \in R^m$, the shape error is

$$\Delta\mathbf{y} = \mathbf{y} - \mathbf{y}_d = \mathbf{R}\mathbf{u} - \mathbf{y}_d. \tag{23}$$

With introduction of proper boundary conditions, the stiffness matrix $\mathbf{K}$ is nonsingular, and therefore, the relationship between the displacement and control voltage can be solved from Eq. (21) as

$$\mathbf{u} = -\mathbf{K}^{-1}\mathbf{g}(\mathbf{v}) + \mathbf{K}^{-1}\mathbf{f}. \tag{24}$$

Substituting Eq. (24) into Eqs. (22) and (23) gives

$$\Delta\mathbf{y} = -\mathbf{R}\mathbf{K}^{-1}\mathbf{g}(\mathbf{v}) + \mathbf{K}^{-1}\mathbf{f} - \mathbf{y}_d = \mathbf{R}\bar{\mathbf{u}} - \mathbf{y}_0, \quad \bar{\mathbf{u}} = -\mathbf{K}^{-1}\mathbf{g}(\mathbf{v}), \qquad \mathbf{y}_0 = \mathbf{y}_d - \mathbf{K}^{-1}\mathbf{f}, \tag{25}$$

where $\bar{\mathbf{u}}$ is the displacement actuated by the control voltage only, and $\mathbf{y}_0$ is the new desired shape including the displacements caused by all mechanical loads. The objective function then is simply defined as the sum of the square errors between the actual shape and the desired shape in any nodes, that is

$$e = |\Delta\mathbf{y}|^2 = (\mathbf{R}\bar{\mathbf{u}} - \mathbf{y}_0)^{\mathrm{T}}(\mathbf{R}\bar{\mathbf{u}} - \mathbf{y}_0). \tag{26}$$

Substituting Eq. (24) into Eq. (26), we have

$$e(\mathbf{v}) = \mathbf{g}^{\mathrm{T}}(\mathbf{v})\mathbf{A}\mathbf{g}(\mathbf{v}) + 2\mathbf{b}^{\mathrm{T}}\mathbf{g}(\mathbf{v}) + \mathbf{y}_0^{\mathrm{T}}\mathbf{y}_0, \tag{27}$$

where

$$\mathbf{A} = \mathbf{K}^{-\mathrm{T}}\mathbf{R}^{\mathrm{T}}\mathbf{R}\mathbf{K}^{-1} \in R^{n\times n}, \quad \mathbf{b} = \mathbf{K}^{-\mathrm{T}}\mathbf{R}^{\mathrm{T}}\mathbf{y}_0 \in R^n. \tag{28}$$

Eq. (27) gives the square error between the actual and desired shapes, which is a function of the nodal displacements and control voltages and serves as the objective function in finding the optimal control voltages in the following sections.

3. Incremental method

To find the optimal control voltage that minimizes the square error expressed in Eq. (27), letting $\partial e(\mathbf{v})/\partial \mathbf{v} = 0$, we have

$$\mathbf{g}^{\mathrm{T}}(\mathbf{v})\mathbf{A}\frac{\partial \mathbf{g}(\mathbf{v})}{\partial \mathbf{v}} + \mathbf{b}^{\mathrm{T}}\frac{\partial \mathbf{g}(\mathbf{v})}{\partial \mathbf{v}} = 0, \tag{29}$$

where $\mathbf{J}(\mathbf{v})\partial \mathbf{g}(\mathbf{v})/\partial \mathbf{v} \in R^{n\times n_V}$ is a Jacobian matrix.

Eq. (29) is a set of nonlinear algebraic equations in terms of the control voltage. When the $\mathbf{v}$ is very close to $\mathbf{v}_0$, introducing the approximations

$$\mathbf{g}(\mathbf{v}) \approx \mathbf{g}(\mathbf{v}_0) + \frac{\partial \mathbf{g}(\mathbf{v}_0)}{\partial \mathbf{v}}(\mathbf{v} - \mathbf{v}_0), \quad \frac{\partial \mathbf{g}(\mathbf{v})}{\partial \mathbf{v}} \approx \frac{\partial \mathbf{g}(\mathbf{v}_0)}{\partial \mathbf{v}} \tag{30}$$

in Eq. (29), gives

$$\left[\mathbf{g}(\mathbf{v}_0) + \frac{\partial \mathbf{g}(\mathbf{v}_0)}{\partial \mathbf{v}}(\mathbf{v} - \mathbf{v}_0)\right]^{\mathrm{T}}\mathbf{A}\frac{\partial \mathbf{g}(\mathbf{v}_0)}{\partial \mathbf{v}} + \mathbf{b}^{\mathrm{T}}\frac{\partial \mathbf{g}(\mathbf{v}_0)}{\partial \mathbf{v}} = 0. \tag{31}$$

To make Eq. (30) hold, the given desired shape function is treated as the sum of many small sub-shapes, that is

$$\mathbf{y}_0 = \sum_{m=1}^{M} \Delta \mathbf{y}_0^m, \tag{32}$$

where $\Delta \mathbf{y}_0^m = \mathbf{y}_0^{m+1} - \mathbf{y}_0^m$ $(m = 1, 2, \ldots, M)$ is the increment of the desired shape. The optimal control voltages to achieve the final desired shape will be obtained step be step by finding the voltages to achieve all the small sub-shapes.

3.1. Simple incremental method (SIM)

To actuate the small increment of the desired shape $\Delta \mathbf{y}_0^m$ from $\mathbf{y}_0^m$, the increment of the optimal control voltages $\Delta \mathbf{v}^m$ from $\mathbf{v}^m$ for the piezoelectric actuator patches can be found from Eq. (31). In each small incremental step, the Jacobian matrix is evaluated at $\mathbf{v}^m$ and the increment of the optimal control voltages $\Delta \mathbf{v}^m$ can be obtained by

$$\Delta \mathbf{b}_m = \mathbf{K}^{-\mathrm{T}}\mathbf{R}^{\mathrm{T}}\Delta \mathbf{y}_0^m, \tag{33}$$

$$\Delta \mathbf{v}^m = -\left[\mathbf{J}^T\mathbf{A}\mathbf{J}(\mathbf{v}^{m-1})\right]^{-1}\mathbf{J}^T(\mathbf{v}^{m-1})\left(\mathbf{A}\mathbf{g}(\mathbf{v}^{m-1}) + \Delta \mathbf{b}_m\right), \tag{34}$$

$$\mathbf{v}^m = \mathbf{v}^{m-1} + \Delta \mathbf{v}^m, \quad m = 1, 2, \ldots, M. \tag{35}$$

The initial control voltage vector $\mathbf{v}^0$ is a zero vector. After M steps, the optimal control voltage $\mathbf{v}^M$ can be obtained, which can actuate a static shape best match the desired shape $\mathbf{y}_0$ for a structures with nonlinear piezoelectric actuators.

3.2. Iterative incremental method (IIM)

To improve the precision of the calculation, the iterative procedure can be employed in each incremental step. In this case, the increment of the control voltages $\Delta\mathbf{v}^m$ for an increment of the desired shape $\Delta\mathbf{y}_0^m$ will be determined iteratively:

$$\Delta\mathbf{b}_m = \mathbf{K}^{-\mathrm{T}}\mathbf{R}^{\mathrm{T}}\Delta\mathbf{y}_0^m, \tag{36}$$

$$\Delta\mathbf{v}_{i+1}^m = \Delta\mathbf{v}_i^m - \left[\mathbf{J}^T\mathbf{A}\mathbf{J}(\mathbf{v}^{m-1}+\Delta\mathbf{v}_i^m)\right]^{-1}\mathbf{J}^T\left(\mathbf{v}^{m-1}+\Delta\mathbf{v}_i^m\right)\left(\mathbf{A}\mathbf{g}(\mathbf{v}^{m-1}+\Delta\mathbf{v}_i^m)+\Delta\mathbf{b}_m\right), \tag{37a}$$

$$\text{Loop for } i \text{ until } \left(\Delta\mathbf{v}_{i+1}^m-\Delta\mathbf{v}_i^m\right)^{\mathrm{T}}\left(\Delta\mathbf{v}_{i+1}^m-\Delta\mathbf{v}_i^m\right) < \varepsilon_0 \text{ then } \Delta\mathbf{v}^m = \Delta\mathbf{v}_{i+1}^m, \tag{37b}$$

$$\mathbf{v}^m = \mathbf{v}^{m-1} + \Delta\mathbf{v}^m, \quad m = 1,2,\ldots,M. \tag{38}$$

The increment of the control voltages obtained from Eqs. (36) to (38) is expected to be more accurate than that obtained from Eqs. (33) to (35) due to the application of the iteration procedure in each incremental step.

3.3. Calibrated incremental method (CIM)

In the SIM given in the previous section, since the desired shape is achieved by implementing many sub-desired-shapes, the error in each incremental step will be passed to the next step due to the fact that the voltages obtained in one step will be used as the base voltage in the next step. The error in every step will be accumulated gradually. Although the iterative procedure employed in each incremental step in the IIM can reduce the error, the accumulated error will not be completely removed. This is because the increment of the control voltages is obtained based on a local desired shape only without any information of the whole shape.

In this section, we presented an improved incremental procedure with overall calibration to find the optima voltages for static shape control of plate with nonlinear piezoelectric actuators. In the method, for the given incremental desired shape $\Delta\mathbf{y}_0^m$, the new obtained control voltage $\tilde{\mathbf{v}}^m = \mathbf{v}^{m-1} + \Delta\mathbf{v}^m$ is treated as an estimation of $\mathbf{v}^m$ (denoted by $\tilde{\mathbf{v}}^m$). $\tilde{\mathbf{v}}^m$ is the approximate control voltage to actuate the desired shape $\mathbf{y}_0^m$. With the estimated value $\tilde{\mathbf{v}}^m$, the nonlinear control forces $\mathbf{g}(\tilde{\mathbf{v}}^m)$ as well as the Jacobian matrix $\mathbf{J}(\tilde{\mathbf{v}}^m)$ can be evaluated. Like a linear system with known piezoelectric stress constant, the optimal control voltages for achieving the given desired shape $\mathbf{y}_0^m$ can be obtained from Eq. (31), that is, $\mathbf{v}^m = -\left[\mathbf{J}^T\mathbf{A}\mathbf{J}(\tilde{\mathbf{v}}^m)\right]^{-1}\mathbf{J}^T(\tilde{\mathbf{v}}^m)(\mathbf{A}\mathbf{g}(\tilde{\mathbf{v}}^m)+\mathbf{b}_m)$. This control voltage serves as the base voltage to calculate the new voltages in the next incremental step. The CIM is described as follows:

$$\Delta\mathbf{b}_m = \mathbf{K}^{-\mathrm{T}}\mathbf{R}^{\mathrm{T}}\Delta\mathbf{y}_0^m, \tag{39}$$

$$\Delta\mathbf{v}^m = -\left[\mathbf{J}^T\mathbf{A}\mathbf{J}(\mathbf{v}^{m-1})\right]^{-1}\mathbf{J}^T(\mathbf{v}^{m-1})(\mathbf{A}\mathbf{g}(\mathbf{v}^{m-1})+\Delta\mathbf{b}_m), \tag{40}$$

$$\tilde{\mathbf{v}}^m = \mathbf{v}^{m-1} + \Delta\mathbf{v}^m, \tag{41}$$

$$\mathbf{b}_m = \Delta\mathbf{b}_1 + \Delta\mathbf{b}_2 + \cdots + \Delta\mathbf{b}_m, \tag{42}$$

$$\mathbf{v}^m = -\left[\mathbf{J}^T\mathbf{A}\mathbf{J}(\tilde{\mathbf{v}}^m)\right]^{-1}\mathbf{J}^T(\tilde{\mathbf{v}}^m)(\mathbf{A}\mathbf{g}(\tilde{\mathbf{v}}^m)+\mathbf{b}_m), \tag{43}$$

$$m = 1,2,\ldots,M.$$

The main difference between the incremental method given in Eqs. (33)–(35) and the CIM in Eqs. (39)–(43) lies in Eqs. (42) and (43), in which a new control voltages $\mathbf{v}^m$ are obtained for the intermediate desired shape $\mathbf{y}_0^m = \sum_{k=1}^m \Delta\mathbf{y}_0^k$ based on its estimation $\tilde{\mathbf{v}}^m$. Since the control voltages $\mathbf{v}^m$ is obtained from the desired shape $\mathbf{y}_0^m$ rather than the incremental desired shape $\Delta\mathbf{y}_0^m$ only, it calibrates the incremental procedure in each step and hence, can improve the precision of the calculation.

3.4. Iteratively-calibrated incremental method (ICIM)

To further improve the accuracy of the calculation, the calibration procedure can be done iteratively by the following iteration process:

$$\Delta\mathbf{b}_m = \mathbf{K}^{-\mathrm{T}}\mathbf{R}^{\mathrm{T}}\Delta\mathbf{y}_0^m, \tag{44}$$

$$\Delta\mathbf{v}^m = -\left[\mathbf{J}^T\mathbf{A}\mathbf{J}(\mathbf{v}^{m-1})\right]^{-1}\mathbf{J}^T(\mathbf{v}^{m-1})(\mathbf{A}\mathbf{g}(\mathbf{v}^{m-1})+\Delta\mathbf{b}_m), \tag{45}$$

$$\tilde{\mathbf{v}}^m = \mathbf{v}^{m-1} + \Delta\mathbf{v}^m, \tag{46}$$

$$\mathbf{b}_m = \Delta\mathbf{b}_1 + \Delta\mathbf{b}_2 + \cdots + \Delta\mathbf{b}_m, \tag{47}$$

$$\tilde{\mathbf{v}}_0^m = \tilde{\mathbf{v}}^m,$$

$$\tilde{\mathbf{v}}_{i+1}^m = -\left[\mathbf{J}^T\mathbf{A}\mathbf{J}(\tilde{\mathbf{v}}_i^m)\right]^{-1}\mathbf{J}^T(\tilde{\mathbf{v}}_i^m)\left(\mathbf{A}\mathbf{g}(\tilde{\mathbf{v}}_i^m)+\mathbf{b}_m\right), \quad i = 1,2,\ldots, \tag{48}$$

$$\text{If } \left|\tilde{\mathbf{v}}_{i+1}^m - \tilde{\mathbf{v}}_i^m\right| < \varepsilon_0 \text{ then } \mathbf{v}^m = \tilde{\mathbf{v}}_{i+1}^m.$$

The main difference between the CIM and the ICIM is that the one-step calibration process in Eq. (43) is replaced by an iterative calibration process in Eq. (48). In this case, the obtained control voltages are also taken as the estimated values, and then use them to find new voltages repeatedly until the control voltages converge.

This incremental procedure not only gives the final control voltages for the desired shape, but also gives the history of the control voltages varying with different desired shapes. Therefore, the advantage of the incremental methods is that it can be applied to the cases where the piezoelectric material has a very complicated behavior such as hysteresis.

4. Illustrative examples

As an example, consider a cantilever rectangular thin plate bonded with 20 nonlinear piezoelectric actuator patches in its upper surface, as shown in Fig. 3. The geometrical dimensions of the structure as well as the mesh are also given in Fig. 3. The host structure is meshed into 99 elements including 79 ordinary plate elements and 20 adhesive elements, and the total node number is 200. Assume that the control voltage is uniformly distributed in each piezoelectric actuator element and no voltage is applied to the host plate. The 20 piezoelectric actuators are numbered as A1–A20 aligned in column order. The total number of electric DOF is $n_V = 20$ and that of the mechanical DOF is $n = 1000$.

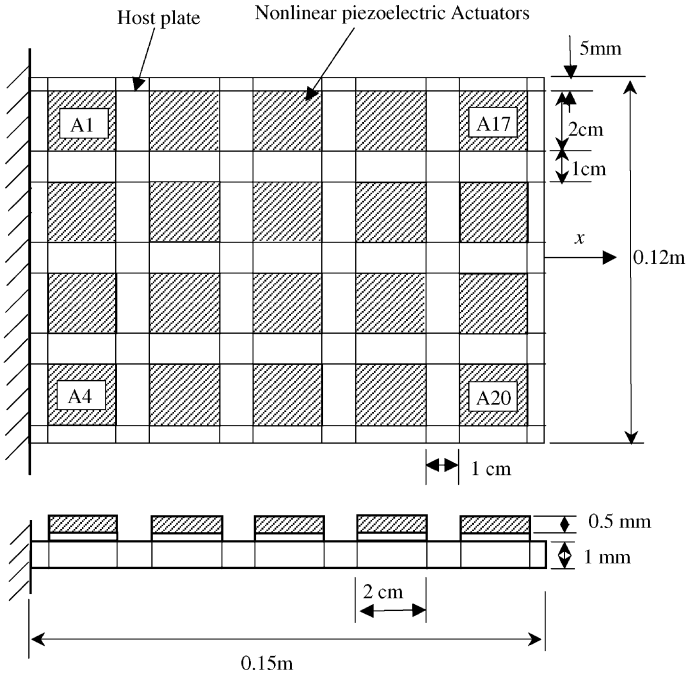

Fig. 3. A cantilevered plate with 20 nonlinear piezoelectric actuators.

The purpose in this example is to find the optimal control voltages to achieve the desired shape of the host plate described by its transverse displacement as follow:

$$w(x,y) = (\cosh x - 1)\sin y/10, \quad 0.0 \leqslant x \leqslant 0.15, \quad -0.06 \leqslant y \leqslant 0.06$$

which represents a twisted shape. In this example, the weighting matrix $\mathbf{R}$ is a 120×1000 matrix and its entries corresponding to the transverse displacements of the host plate are set to 1.0 and other entries zero so that the generalized shape $\mathbf{y}$ is composed of only the transverse displacements at all nodes of the host plate only.

In the following calculation, the host plate is made of isotropic aluminum and the piezoelectric actuators are made of piezoelectric ceramic PZT. The Young's moduli of the host plate, the piezoelectric material and the adhesive layer are 68.9, 81.3 and 2.4 GPa, respectively. The Poisson's ratios of these materials are 0.25, 0.43 and 0.34, respectively. The piezoelectric stress modulus of the piezoelectric material is a function of the applied control voltage (field). In practice, the nonlinear function of a given piezoelectric material can be obtained from its tested strain–field curve. In this example, to demonstrate the proposed incremental algorithms for finding the control voltage of nonlinearly actuated structure, we simply choose the piezoelectric stress modulus as

$$e_{31}\ (\mathrm{V}) = e_{32}\ (\mathrm{V}) = e_0[1 + \alpha\ \mathrm{sgn}\ (\mathrm{V})V] \tag{49}$$

and the other entries in the piezoelectric stress matrices $\mathbf{e}_{b1}$ and $\mathbf{e}_{s1}$ are zero. The parameter α in Eq. (49) is a nonlinear factor which determines the shape of the nonlinear stress–voltage curve. A negative nonlinear factor α represents a softening nonlinear stress–voltage relationship. Fig. 4 gives the nonlinear relationship between the induced stress and the applied control voltage for different α with $e_0 = 9.53$ N/V m.

First, the incremental method with and without iteration are examined by comparing with the feedback algorithm (FA) given by Ajit et al. (2001). When $e_0 = -9.53$ N/V m, $\alpha = -1 \times 10^{-4}$ in Eq. (44) and

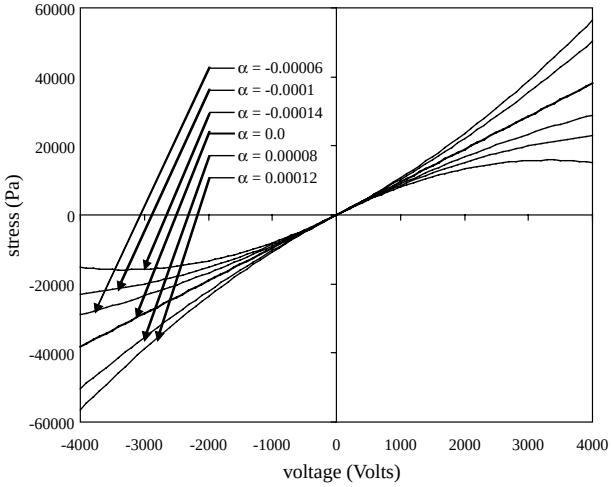

Fig. 4. Nonlinear stress–electric field curve.

$\varepsilon_V = 10^{-5}$, the optimal control voltage distribution to achieve the desired shape is obtained by FA and listed in Table 1, which is used as the baseline of the comparison.

To use the incremental method, the desired shape is divided into 20 equal incremental shapes, and the optimal control voltages are calculated using the algorithm given in Eqs. (33)–(35) after 20 steps and

Table 1
Optimal control voltages (V) obtained by different algorithms

Actuators	FA (Ajit et al., 2001)	Method							
		SIM		IIM		CIM		ICIM	
		Voltage (V)	Error (%)	Voltage (V)	Error (%)	Voltage (V)	Error (%)	Voltage (V)	Error (%)
A1	−1000.9	−942.95	−5.79	−947.89	−5.30	−1000.14	−0.08	−1000.9	0
A2	−1337.52	−1230.54	−8.00	−1239.26	−7.35	−1335.39	−0.16	−1337.52	0
A3	1337.52	1230.54	−8.00	1239.26	−7.35	1335.39	−0.16	1337.52	0
A4	1000.9	942.95	−5.79	947.89	−5.30	1000.14	−0.08	1000.9	0
A5	−2357.54	−1989.76	−15.60	−2014.93	−14.53	−2337.52	−0.85	−2357.54	0
A6	1299.8	1199.15	−7.74	1207.39	−7.11	1297.89	−0.15	1299.8	0
A7	−1299.8	−1199.15	−7.74	−1207.39	−7.11	−1297.89	−0.15	−1299.8	0
A8	2357.54	1989.76	−15.60	2014.93	−14.53	2337.52	−0.85	2357.54	0
A9	−1540.14	−1395.42	−9.40	−1406.85	−8.65	−1536.55	−0.23	−1540.14	0
A10	889.09	843.87	−5.09	847.78	−4.65	888.58	−0.06	889.09	0
A11	−889.09	−843.87	−5.09	−847.78	−4.65	−888.58	−0.06	−889.09	0
A12	1540.14	1395.42	−9.40	1406.85	−8.65	1536.55	−0.23	1540.14	0
A13	−1367.69	−1255.5	−8.20	−1264.6	−7.54	−1365.39	−0.17	−1367.69	0
A14	569.56	551.57	−3.16	553.19	−2.87	569.45	−0.02	569.56	0
A15	−569.56	−551.57	−3.16	−553.19	−2.87	−569.45	−0.02	−569.56	0
A16	1367.69	1255.5	−8.20	1264.6	−7.54	1365.39	−0.17	1367.69	0
A17	197.88	195.78	−1.06	195.98	−0.96	197.87	−0.01	197.88	0
A18	187.77	185.88	−1.01	186.06	−0.91	187.76	−0.01	187.77	0
A19	−187.77	−185.88	−1.01	−186.06	−0.91	−187.76	−0.01	−187.77	0
A20	−197.88	−195.78	−1.06	−195.98	−0.96	−197.87	−0.01	−197.88	0
Square error (m^2)	1.2647×10^{-9}	1.5878×10^{-9}		1.5478×10^{-9}		1.2652×10^{-9}		1.2647×10^{-9}	

presented in Table 1. To improve the accuracy of the increment of the control voltages in each incremental step, the method in Eqs. (36)–(38) is used and the obtained control voltage is also listed in Table 1. It is found that the control voltages of the actuators are anti-symmetrical about the x-axis, and actuator A5 and A8 have the highest voltage.

Table 1 shows that the SIM in Eqs. (33)–(35) can only give a rough estimation of the optimal control voltage distribution for the static shape control with nonlinear piezoelectric actuators. Compared to the results obtained from FA, the maximum error of the control voltages in Table 1 is 15.6%. When the IIM in Eqs. (36)–(38) is used to determine the incremental voltages for each given increment of the desired shape, the obtained final control voltages can be improved, the relative maximum error is reduced to 14.5%. It is found that the error of the obtained control voltage distribution using the incremental method cannot be remarkably decreased by increasing the number of incremental steps. Therefore, both SIM and IIM are not competent methods to find the control voltages in nonlinear shape control of structures.

Next, the effectiveness of the CIM is evaluated. When the desired shape is still divided into 20 equal incremental shapes, the control voltages can be calculated using CIM method given in Eqs. (39)–(43) and listed in Table 1. The results have been significantly improved compared to the simple incremental algorithm. For example, the maximum error in the voltages obtained by the CIM is less than 0.85%. If the number of the incremental steps is increased, more accurate control voltages can be obtained using this method. In addition, when the ICIM is used, the deviation of the control voltage can be completely removed, as shown in Table 1.

Fig. 5 gives the history of the control voltages of the actuator patch A5, which has the highest control voltage, with the different intermediate desired shapes. In Fig. 5, the λ_m represents the intermediate desired shapes such that $\mathbf{Y}_0^m = \lambda_m \mathbf{Y}_0$. As shown in Fig. 5, the error of the control voltage obtained by the SIM and IIM become increasingly larger as the desired displacements increase. However, the CIM can give a satisfactory estimation of the control voltage as long as the number of the total incremental steps is adequate. The ICIM method can give the same results as the FA. Therefore, in the following calculations, only the ICIM method in Eqs. (44)–(48) is employed.

Applying the obtained the optimal control voltages to the nonlinear piezoelectric actuators, we can obtain the actually achieved shape. Fig. 6 presents the transverse displacements at all nodes and Fig. 7 gives the overall view of the actuated shape and the desired shape. It is can be seen from Figs. 6 and 7 that the achieved shape is very closed to the desired one and the square error between the actuated shape and the desired one is 1.26×10^{-9} m^2.

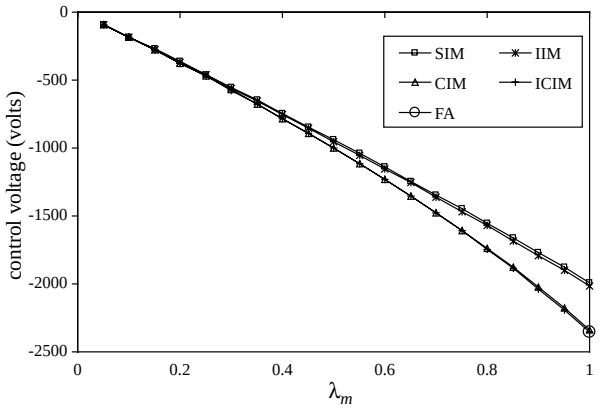

Fig. 5. History of the control voltage on actuator A5 with different intermediate desired shapes.

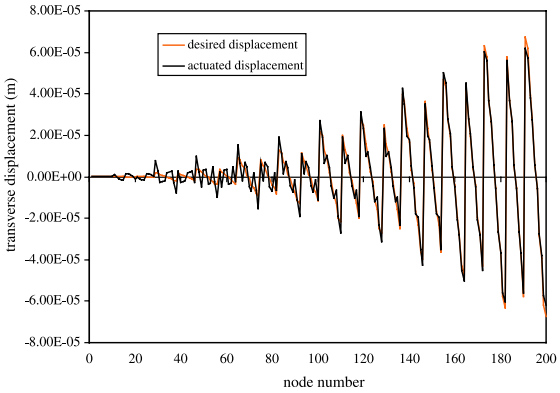

Fig. 6. The actuated and desired transverse displacements at all nodes of the host plate.

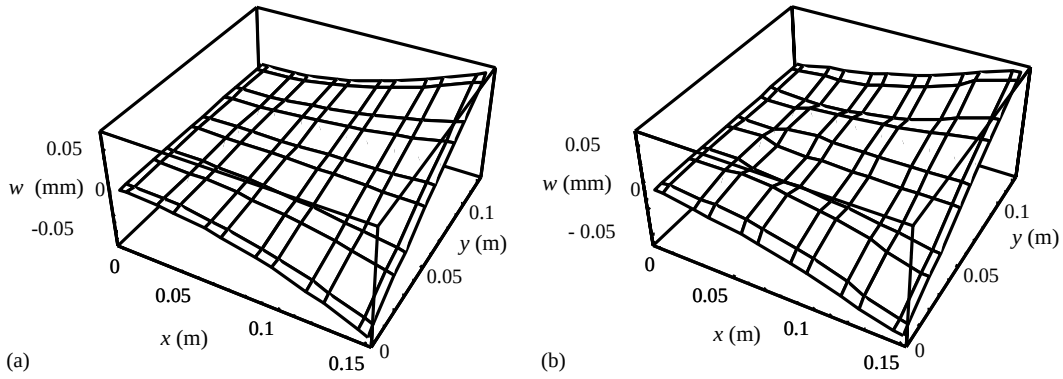

Fig. 7. The actuated shape (a) and the desired shape (b).

The main advantage of the incremental method is that it can give a history of the control voltages as the desires shape approaches to the final one although more CPU time is needed than FA in the calculation. Fig. 8 presents the history of the control voltages on the actuators with positive voltages when $\alpha = -1 \times 10^{-4}$. It shows that the optimal control voltage on each actuator increases nonlinearly as the shape approaches to the desired one, particularly for those with higher control voltages such as actuator A8 and A12. In this case, the final control voltage on actuator A8 is 31% higher than that for the linear case ($\alpha = 0$).

Next, the effect of the nonlinear piezoelectricity on the optimal voltage distribution is examined. The history of the control voltage on actuator A8 is calculated and shown in Fig. 9 using the ICIM method for different nonlinear factor α from 0 to -0.00012, which represents a weakening nonlinearity. As indicated in this figure, the control voltage in the actuator requested to achieve a given transverse displacement distribution varies nonlinearly as the desired displacement gets larger. The stronger the nonlinearity of the piezoelectricity of the piezoelectric material is, the more significant the rate of change of the control voltage with respect to desired shape. Fig. 10 depicts the relationship between the control voltage distribution on all actuators and the nonlinearity of the piezoelectricity. Since the obtained optimal voltages are anti-symmetrical about the axis x, only the positive ones are presented in Fig. 10 for different nonlinear factors.

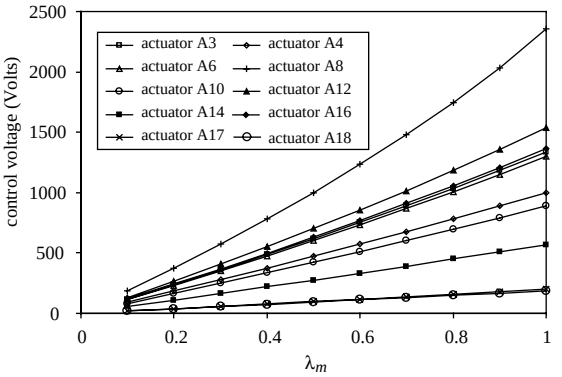

Fig. 8. History of control voltages as the shape approaches the desired one.

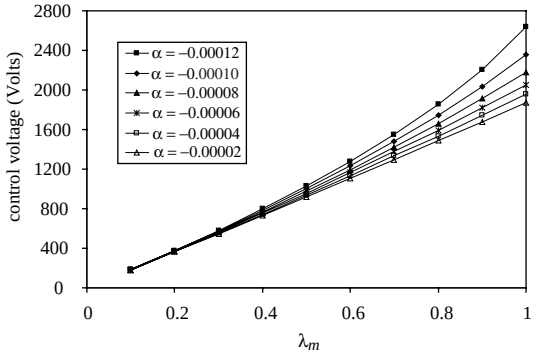

Fig. 9. Effect of nonlinearity of the piezoelectricity on the history of the optimal control voltage on actuator A8.

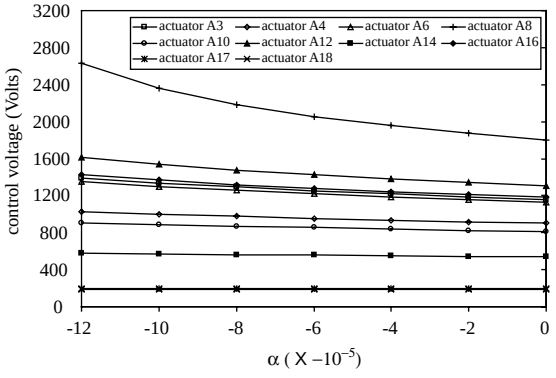

Fig. 10. Effect of nonlinearity of the piezoelectricity on the distribution of the optimal control voltages.

Fig. 10 shows that the optimal control voltage for each piezoelectric actuator become higher as the nonlinear factor α decreases. The increases of the control voltages due to the weakening nonlinearity of the piezoelectricity are more remarkable for the actuators with higher control voltages than those with lower

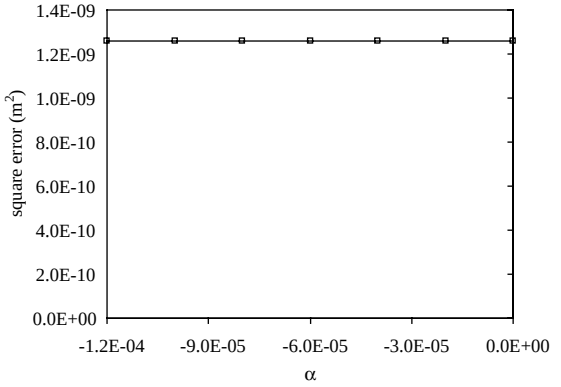

Fig. 11. Effect of nonlinearity of the piezoelectricity on the square error.

voltages. For instance, the nonlinearity with $\alpha = -0.00012$ makes the control voltage on actuator A8 increase 46.2% than that in the linear case. However, the same nonlinearity causes an increase of 2.4% in the voltage on actuator A17. In the calculation, it is observed that the optimal control voltages cannot be obtained using any methods when $\alpha < -0.00015$. The reason is that increasing the voltage on some actuator which needs high voltage will no longer provide any more actuating forces due to the softening nonlinear stress–voltage relationship.

Finally, it should be mentioned that the square error between the achieved shape and the desired one does not depend on the nonlinear factor α, as shown in Fig. 11. The shape achieved by the nonlinear piezoelectric actuators with the optimal control voltages is the same as that by the nonlinear ones with their corresponding control voltages.

5. Conclusions

Based on an eight-node adhesive element including a pair of collocated four-node quadrilateral elements for the upper and lower adherents and a pseudo-adhesive layer element, static shape control of structures with nonlinear piezoelectric actuators is investigated. An iteratively calibrated incremental algorithm is presented to find the optimal control voltages. In this method, the desired shape is expressed by the sum of a number of small incremental desired shapes, and the control voltages to achieve each incremental desired shape are calculated step by step. The control voltages in each step then are calibrated by using the accumulated intermediate desired shape. Finally, a simulation example is given to illustrate the effectiveness of the present algorithm in finding the optimal control voltage distribution for shape control of nonlinearly actuated structures. Comparison with the feedback algorithm shows that this method can give accurate control voltages.

Acknowledgements

The authors are grateful to the support of the Australian Research Council via Discovery-Projects Grant (Grant No. DP0210716) and the National Natural Foundation of China (Grant No. 60034010).

References

Agnes, G.S., Inman, D.J., 1996. Nonlinear piezoelectric vibration absorbers. Smart Materials and Structures 5 (5), 704–714.

Agrawal, B.N., Treanor, K.E., 1999. Shape control of a beam using piezoelectric actuators. Smart Materials and Structures 8 (6), 729–739.

Ajit, A., Ang, K.K., Wang, C.M., 2001. Shape control coupled nonlinear piezoelectric beams. Smart Materials and Structures 10, 914–924.

Benjeddou, A., Trindade, M.A., Ohayon, R., 1999. New shear actuated smart structure beam finite element. AIAA Journal 37 (3), 378–383.

Bruch, J.C., Sloss, J.M., Adali, S., Sadek, I.S., 2000. Optimal piezo-actuator locations/lengths and applied voltage for shape control of beams. Smart Materials and Structures 9 (2), 205–211.

Chee, C., Tong, L., Steven, G.P., 2001. Static shape control of composite plates using a curvature-displacement based algorithm. International Journal of Solids and Structures 38 (36–37), 6381–6403.

Chee, C., Tong, L.Y., Steven, G.P., 2002. Static shape control of composite plates using a slope-displacement-based algorithm. AIAA Journal 40 (8), 1611–1618.

Crawley, E.F., Lazarus, K.B., 1991. Induced strain actuation of isotropic and anisotropic plates. AIAA Journal 29, 944–951.

Ghosh, K.G., Batra, R.C., 1995. Shape control of plates using piezoceramic elements. AIAA Journal 33 (7), 1354–1357.

Hsu, C.Y., Lin, C.C., Gaul, L., 1997. Shape control of composite plates by bonded actuators with high performance configuration. Journal of Reinforced Plastics and Composites 16 (18), 1692–1710.

Irschik, H., 2002. A review on static and dynamic shape control of structures by piezoelectric actuation. Engineering Structures 24, 5–11.

Koconis, D.B., Kollar, L.P., Springer, G.S., 1994. Shape control of composite plates and shells with embedded actuators. 2. Desired shape specified. Journal of Composite Materials 28 (5), 459–482.

Tan, P., Tong, L., 2001. Micromechanics models for nonlinear behavior of piezoelectric fiber reinforce composite materials. International Journal of Solids and Structures 38, 8999–9032.

Tong, L.Y., Sun, X.N., 2000. Stress analysis of bonded and curved lap joints. In: Ochoa, O.O. (Ed.), Proceedings of American Society Composites 15th Technical Conference, Texas A&M University, USA, pp. 719–728.

Tong, D.Q., Williams II, R.L., Agrawal, S.K., 1998. Optimal shape control of composite thin plates with piezoelectric actuators. Journal of Intelligent Material Systems and Structures 9, 458–467.

Vel, S.S., Batra, R.C., 2001. Exact solution for the cylindrical bending of laminated plates with embedded piezoelectric shear actuators. Smart Materials and Structures 10 (2), 240–251.

Wang, Q.M., Zhang, Q.M., Xu, B.M., Liu, R.B., Cross, L.E., 1999. Nonlinear piezoelectric behavior of ceramic bending mode actuators under strong electric fields. Journal of Applied Physics 86 (6), 3352–3360.

Zhang, X.D., Sun, C.T., 1999. Analysis of a sandwich plate containing a piezoelectric core. Smart Materials and Structures 8 (1), 31–40.

Zhou, H., Chattopadhyay, A., 2001. Hysteresis behavior and modeling and piezoceramic actuators. Journal of Applied Mechanics 68, 270–277.

Zhou, Y.H., Tzou, H.S., 2000. Active control of nonlinear piezoelectric circular shallow spherical shells. International Journal of Solids and Structures 37 (12), 1663–1677.